

Transition Metals

Periodic Trends in the Binding of a Phosphine-Tethered Ketone Ligand to Fe, Co, Ni, and Cu

Dide G. A. Verhoeven,^[a] Maxime A. C. van Wiggan,^[a] Joost Kwakernaak,^[a] Martin Lutz,^[b] Robertus J. M. Klein Gebbink,^[a] and Marc-Etienne Moret^{*[a]}

Abstract: π -Coordinating ligands are commonly found in intermediate structures in homogeneous catalysis, and are gaining interest as supporting ligands for the development of cooperative catalysts. Herein, we systematically investigate the binding of the ketone group, a strongly accepting π ligand, to mid-to-late metals of the first transition series. To this end, the coordination of 2,2'-bis(diphenylphosphino)-benzophenone (^{Ph}dppb), which features a ketone moiety flanked by two strongly binding P-donor groups, to Fe, Co, Ni, and Cu was explored. The ketone moiety does not bind

to the metal in M^{II} complexes, whereas M^I complexes (Fe, Co, Ni) adopt an $\eta^2(C,O)$ coordination. A structural and computational investigation of periodic trends in this series was performed. These data suggest that the coordination of the ketone to M^I can mostly be described by the resonance extremes of the Dewar–Chatt–Duncanson model, that is, the π complex and the metallaoxacycle extreme, with a possible minor contribution from a ketyl radical resonance structure in the case of the iron complex.

Introduction

The coordination of π ligands is of paramount importance in organometallic chemistry and transition-metal catalysis. The π complexes of carbon–carbon and carbon–heteroatom multiple bonds are reactive intermediates in a large number of catalytic reactions, which includes hydrogenations, hydrofunctionalizations, oligo- and polymerizations.^[1–3] In addition, incorporation of such moieties in multidentate ligand architectures is a promising approach to cooperative ligand design.^[4]

The polarity of the carbon–oxygen double bonds in aldehydes and ketones sets them apart amongst π -binding ligands. The C=O bond can bind to transition metals through either an $\eta^1(O)$ -interaction based on σ -donation, which is allowed by the presence of oxygen-centered lone-pairs, or through a π -coordinating $\eta^2(C,O)$ interaction. The latter, less common binding mode has been proposed in intermediate structures for the Cu-catalyzed addition of Grignard reagents,^[5,6] Ru-catalyzed hydrogenation reactions,^[7,8] and oxidative addition of arylketone C–C bonds.^[9–11] In particular, Piers and co-workers recently re-

ported a remarkable oxygen atom transfer from N_2O to an Ir=C double bond to yield an iridaepoxide complex that serves as an intermediate in the formal hydrogenation of N_2O to N_2 and H_2O .^[12] The Ir–(C–O) motif was described as the intermediate between an η^2 ketone complex (Ir^{III}) and an iridaepoxide (Ir^V) structure.^[13,14] Seeking a direct access to ketone-based π complexes of first-row transition metals, we recently investigated the coordination chemistry of the diphosphine–ketone ligand 2,2'-bis(diphenylphosphino)benzophenone^[8] (^{Ph}dppb, **1**) with nickel (Scheme 1).^[15] The ketone moiety does not bind to the $Ni^{II}Cl_2$ fragment but binds in an $\eta^2(C,O)$ fashion upon reduction of the nickel center from Ni^{II} to Ni^I or Ni^0 ; hence, it acts as a hemilabile acceptor ligand.

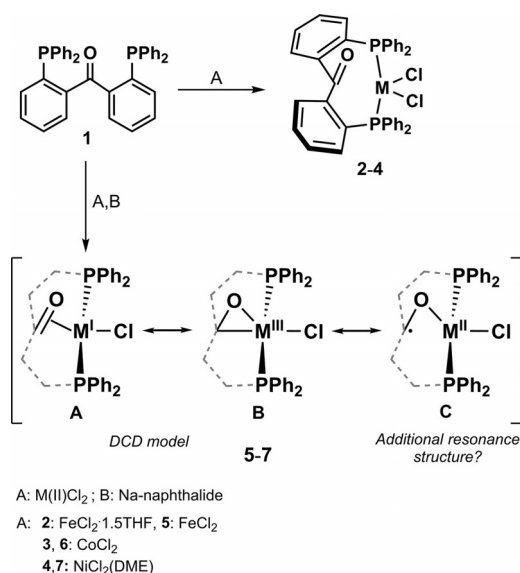
Side-on binding is generally favored by electron-rich metal centers and can be described by the Dewar–Chatt–Duncanson (DCD) model for π -coordinating ligands: the bond is established by electron donation from a filled π orbital (σ donation) and simultaneous donation of d electrons from the metal to the π antibonding orbital (π backbonding).^[16,17] The latter process is expected to dominate the binding of the C=O moiety, because the high electronegativity of the oxygen atom lowers the energy of both the π and π^* orbitals, which results in net charge transfer from the metal to the ligand upon binding. In addition, the larger C coefficient of the accepting $\pi^*(C=O)$ orbital should result in a strengthening of the M–C bond as backdonation increases.^[18] The DCD model can also be expressed in terms of two resonance structures: the π complex (Scheme 1A) and the metallaoxacycle (Scheme 1B) extreme, which leads to ambiguity over the oxidation state of the complex (M^n or M^{n+2}).

Herein, we describe a systematic study of the coordination of the ketone moiety in ^{Ph}dppb to mid-to-late metals of the

[a] D. G. A. Verhoeven, M. A. C. van Wiggan, J. Kwakernaak, Prof. Dr. R. J. M. Klein Gebbink, Dr. M.-E. Moret
Organic Chemistry and Catalysis, Debye Institute for Nanomaterials Science
Faculty of Science, Utrecht University
Universiteitsweg 99, 3584 CG, Utrecht (The Netherlands)
E-mail: m.moret@uu.nl

[b] Dr. M. Lutz
Crystal and Structural Chemistry, Bijvoet Center for Biomolecular Research
Faculty of Science, Utrecht University
Padualaan 8, 3584 CG, Utrecht (The Netherlands)

Supporting information and the ORCID identification number(s) for the author(s) of this article can be found on the WWW under <https://doi.org/10.1002/chem.201703254>.



Scheme 1. Synthesis of base metal complexes **2–7**. Resonance structures: the side-on bound extreme **A** (M^I), the metalla-oxocycle extreme **B** (M^{III}) of the DCD model, and the additional ketone radical extreme **C** ($[M^I]$).

first transition series: Fe, Co, Ni, and Cu. The rigid phenylene linkers and the strong phosphine donor groups in the $^{Ph}dpbp$ ligand are suitable for $\eta^2(C,O)$ coordination of the ketone but disfavor $\eta^1(O)$ coordination, which makes this ligand an ideal platform to study the former mode in detail. Indeed, the ketone group in $^{Ph}dpbp$ is not bound in complexes of the $M^II Cl_2$ fragments ($M = Fe, Co, Ni$), as evidenced by $M-C$ and $M-O$ distances above 3 Å, even though some evidence for a weak residual interaction arises from $C-O$ bond lengths and the corresponding IR absorption frequencies. In contrast, $\eta^2(C,O)$ coordination occurs with the more reduced $M^I Cl$ fragment ($M = Fe, Co, Ni$), which results in high-spin pseudotetrahedral $(^{Ph}dpbp)MCl$ complexes. Structural and computational analysis of the series indicates that increased charge transfer to the ketone moiety from the metal center in the sequence Ni to Fe correlates with stronger $M-O$ bonding and weaker $M-C$ bonding. Whereas the $\eta^2(C,O)$ coordination of the ketone is mostly described by the covalent DCD model, the observed trend appears to be in disagreement with the large C coefficient of the accepting $\pi^*(C=O)$ orbital in this model. A possible way to resolve this apparent discrepancy is by consideration of a minor contribution of a third resonance structure (Scheme 1 C), which arises from the interaction of a ketyl radical anion with a high-spin M^II center.

Results and Discussion

$M^II Cl_2$ complexes

The coordination chemistry of the $^{Ph}dpbp$ ligand (**1**) with Fe^{II} and Co^{II} centers was investigated: the reaction of ligand **1** with $FeCl_2 \cdot 1.5THF$ or $CoCl_2$ in THF followed by precipitation with hexanes afforded the high-spin complexes $(^{Ph}dpbp)FeCl_2$ (**2**) and $(^{Ph}dpbp)CoCl_2$ (**3**), respectively (Figures 1 and 2). 1H NMR

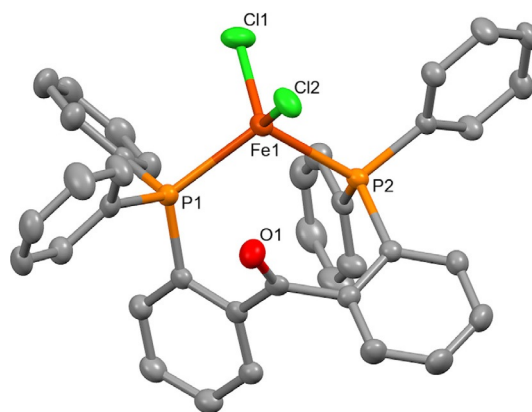


Figure 1. X-ray crystal structure of $(^{Ph}dpbp)FeCl_2$ (**2**). A co-crystallized toluene molecule and hydrogen atoms are omitted for clarity; ellipsoids are shown at 50% probability level. Selected bond lengths (Å) and angles ($^\circ$): $Fe1-O1$: 2.9414(17), $Fe1-C7$: 3.353(7), $Fe1-P1$: 2.4918(7), $Fe1-P2$: 2.5055(6), $Fe1-Cl1$: 2.2355(7), $Fe1-Cl2$: 2.2487(7), $P1-Fe1-P2$: 105.32(2), dihedral angle between phenyl rings: 65.18(11).

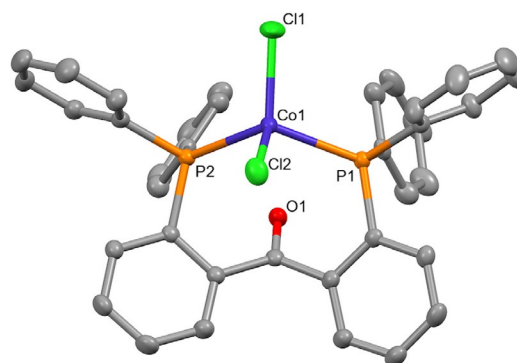


Figure 2. X-ray crystal structure of $(^{Ph}dpbp)CoCl_2$ (**3**). A co-crystallized THF molecule and hydrogen atoms are omitted for clarity; ellipsoids are shown at 50% probability level. Selected bond lengths (Å) and angles ($^\circ$): $Co1-O1$: 2.9255(13), $Co1-C7$: 3.2896(18), $Co1-P1$: 2.3908(5), $Co1-P2$: 2.4059(5), $Co1-Cl1$: 2.1980(6), $Co1-Cl2$: 2.2238(5), $P1-Co1-P2$: 116.676(18), dihedral angle between phenyl rings: 36.16(9).

signals that range from -1.4 to 14.1 and -3.7 to 18.7 ppm for products **2** and **3**, respectively, indicate the formation of paramagnetic complexes. The high spin state ($S=3/2$) of cobalt in complex **3** was further confirmed by an effective magnetic moment (μ_{eff}) of $4.1 \mu_B$ (Evans' method).^[19] Single-crystal X-ray structure determinations of complexes **2** and **3** revealed that both exhibit a distorted tetrahedral geometry around the M^{II} center without coordination of the $C=O$ moiety, which is analogous to the previously reported $(^{Ph}dpbp)NiCl_2$ complex (**4**).^[15]

A systematic comparison of the series of compounds **2–4** provides further insight into the interaction between the unbound $C=O$ fragment and the metal. Even though the $C=O$ moiety is not bound, a consistent trend is observed in the $C=O$ bond lengths of the three complexes; starting from 1.213(3) Å in the free ligand,^[8] the $C-O$ distance gradually increases to 1.2288(16) Å upon complexation to more electron-rich metallic centers (Fe^{II} , Co^{II} , and Ni^{II}) (Table 1). A similar trend was found for the bands in ATR-IR spectroscopy; the $C=O$

Table 1. Selected bond lengths, angles, and IR frequencies for complex 1 and $(^{\text{Ph}}\text{dppb})\text{M}^{\text{II}}$ complexes.

	C=O [Å]	O–M [Å]	PMP angle [°]	IR freq C=O [cm ^{−1}]
$^{\text{Ph}}\text{dppb}$ (1)	1.213(3) ^[8]	–	–	1661
$(^{\text{Ph}}\text{dppb})\text{FeCl}_2$ (2)	1.218(3)	2.9414(17)	105.32(2)	1651
$(^{\text{Ph}}\text{dppb})\text{CoCl}_2$ (3)	1.227(2)	2.9255(13)	116.676(18)	1647
$(^{\text{Ph}}\text{dppb})\text{NiCl}_2$ (4) ^[15,21]	1.2288(16)	3.1012(10)	112.996(13)	1634

band of the free ligand is observed at 1661 cm^{−1}, and this shifts towards lower energy upon complexation to Fe (1651 cm^{−1}), Co (1647 cm^{−1}), and Ni (1634 cm^{−1}).^[15]

Both of these trends suggest that the C=O bond is increasingly, although only slightly, weakened upon the complexation of $^{\text{Ph}}\text{dppb}$ to Fe, Co, and Ni. A first hypothesis to explain this trend is that the decreasing size of the metal ion would result in a gradual conformational change around the C=O; however, the absence of a systematic trend in the P–M–P angle argues against this interpretation. Hence, we favor the presence of an electronic metal–ketone interaction either a) through space by residual orbital overlap or b) through bonds by inductive effects. This question is further addressed on the basis of structural considerations and DFT calculations at the B3LYP/TZVP level of theory (Table 2). First, the sum-of-angles around the

Table 2. Wiberg bond indices (WBI), natural charges (q), and natural spin densities (NSD) from calculated densities at the B3LYP/TZVP level for the ligand and the M^{II} complexes.

	1 ($^{\text{Ph}}\text{dppb}$)	2 (Fe^{II})	3 (Co^{II})	4 (Ni^{II})
WBI(C–O)	1.78	1.80	1.71	1.71
WBI(M–O)	–	< 0.01	< 0.01	< 0.01
WBI(M–C)	–	< 0.01	< 0.01	< 0.01
q(C)	0.56	0.54	0.54	0.54
q(O)	−0.52	−0.48	−0.53	−0.53
q(C+O)	0.04	0.06	0.01	0.02
NSD(M)	–	3.61	2.56	1.51

central C=O carbon atom of complexes 2–4 remains close to 360° throughout the series (2: 359.99°, 3: 359.44°, 4: 359.64°), which indicates negligible rehybridization. In addition, M–O and M–C Wiberg bond indices (WBI) that are consistently below 0.01 indicate the absence of significant covalent bonding. In all cases, the C–O bond index was close to the value for the free ligand (1.7–1.8 e), which indicates that this bond retains its double bond character. In agreement, the calculated natural charge on the ketone fragment q(C+O) hardly deviates from that of the free ligand. Finally, an Atoms-In-Molecules (AIM) analysis^[20] does not identify a bonding pathway between the ketone moiety and the metal center (see the Supporting Information, Figures S28–S33). Considered collectively, these calculated data rule out a covalent bonding interaction between the metal and the ketone moiety. Hence, we tentatively attribute the observed trend in the C=O bond length and IR absorption frequency to through-bond inductive effects, the

ketone moiety being maintained in proximity of the metal by the rigid phenylene linkers. Next, we investigated whether coordination could be induced by either halide abstraction (making the metal more electrophilic) or reduction (making the metal more electron-rich).

Halide abstraction

The abstraction of a halide ligand is a common strategy to induce binding of a hemilabile moiety,^[22–25] as was recently demonstrated by Iluc for the central olefin of diphosphine-substituted *trans*-stilbene ligands.^[23] To probe whether coordination of the C=O moiety could be facilitated in the same way, we investigated halide abstraction from the nickel complex $(^{\text{Ph}}\text{dppb})\text{NiCl}_2$ (4). Compound 4 and $\text{NaB}(\text{Ar}^{\text{F}})_4$ (Ar^{F} = 3,5-bis(trifluoromethyl)phenyl) were mixed in Et₂O and stirred overnight. Subsequent precipitation of the product from Et₂O/hexanes followed by extraction with Et₂O resulted in the diamagnetic Ni^{II} complex 8. The ¹H NMR spectrum of product 8 shows sharp aromatic signals at 6–8 ppm and four broadened aromatic peaks. Analysis by ¹³C NMR shows the presence of the carbonyl moiety as a triplet signal at 206.8 ppm (³J_{CP} = 2.9 Hz). This is further confirmed by ATR-IR analysis, which displays a band at 1525 cm^{−1}. Both of these observations indicate that an η²(C,O) interaction is not present. The shift of the C=O vibration by −109 cm^{−1} in the IR spectrum is relatively large and is expected to be caused by an η¹(O) interaction to nickel.^[26] The ³¹P NMR spectrum contains two singlet signals at 5.6 and 36.4 ppm, which are consistent with the presence of both an unbound phosphine and a metal-coordinated phosphine, respectively.^[27] 2D NMR analysis by ¹H–³¹P HMBC NMR and ¹H–¹H zTOCSY are consistent with these results (see the Supporting Information, Figure S12). Together, these findings suggest that the diphosphine–ketone ligand binds in a chelating κ²(P,O) fashion. This structural motif has been previously documented in, for example, the synthesis of nickel complexes as chelating κ²(P,O) ligands for ethylene oligomerization and polymerization reactions, which used 2-(diphenylphosphine)benzoic acid or its methyl ester analogue.^[26–30] The B(Ar^F)₄ counterion was observed in ¹¹B and ¹⁹F NMR at −6.6 and −62.9 ppm, respectively.^[23] Furthermore, the atom composition of the complex was confirmed by elemental analysis.

Overall, the collected data suggests the successful synthesis of a dimeric structure in which two monomers are bound through two bridging chloride atoms in the form $[\text{Ni}(^{\text{Ph}}\text{dppb})(\mu\text{-Cl})_2(\text{B}(\text{Ar}^{\text{F}})_4)_2]$ (8) (Figure 3),^[32,33] which is analogous to the $[\text{Ni}(\text{dtpbe})(\mu\text{-Cl})_2(\text{B}(\text{Ar}^{\text{F}})_4)_2]$ (dtpbe = 1,2-bis(di-*tert*-butylphosphino)ethane) complex that was reported by Hey-Hawkins and co-workers.^[34] Compound 8 eluded structural characterization by X-ray crystallography; therefore, the proposed structure was investigated by DFT calculations at the B3LYP/6-31G** level of theory (Figure 3). These calculations predict a frequency shift of −129 cm^{−1} between compound 4 and 8, which is in line with the observed shift of −109 cm^{−1}. Comparison of the dimeric structure with a possible monomer showed an energy difference of 41 kcal mol^{−1}, which favors the dimeric structure with the incorporated η¹(O) binding mode.

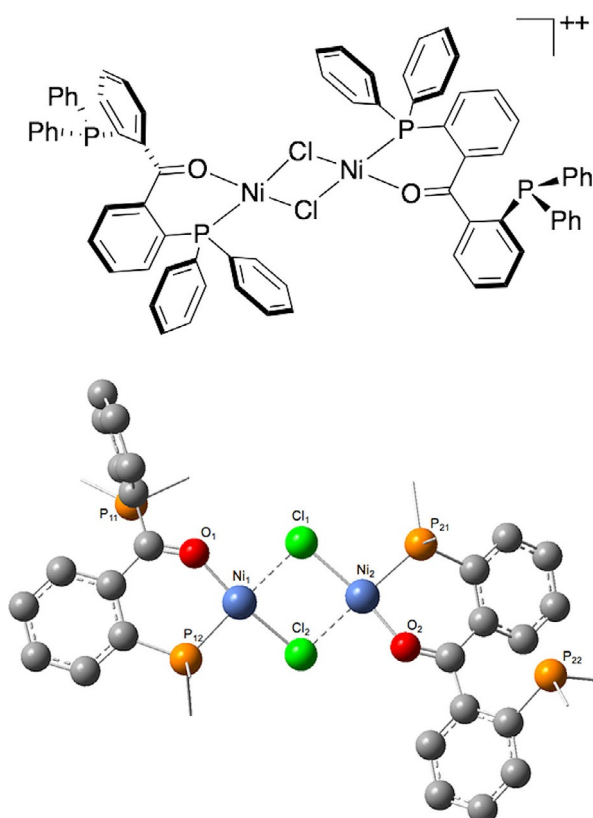


Figure 3. Structure of the dimeric $\text{Ni}^{\text{II}+}$ complex **8**: schematic representation (top) and the structure as calculated with DFT at the B3LYP/6-31G** level of theory (bottom), all hydrogen atoms and the phenyl substituents on the phosphorus atom were left out for clarity.

Similar experiments were performed with $\text{Fe}^{\text{II-}}$ and $\text{Co}^{\text{II-}}$ -based complexes **2** and **3**, but unfortunately led to intractable mixtures of products.

$\text{M}^{\text{I}}\text{Cl}$ complexes

As π coordination is generally favored by more electron-rich metal centers, we investigated the ability of the ketone moiety of the $^{\text{Ph}}\text{dppb}$ ligands to undergo $\eta^2(\text{C},\text{O})$ coordination to the metals in reduced oxidation states. A series of Fe, Co, and Cu analogues of the previously reported $(^{\text{Ph}}\text{dppb})\text{NiCl}$ are presented herein, and trends in the properties of these complexes are discussed.

A reduced iron complex was obtained upon addition of sodium naphthalide to a solution of complex **2**, which was generated in situ from FeCl_2 and $^{\text{Ph}}\text{dppb}$ in THF. The product $(^{\text{Ph}}\text{dppb})\text{FeCl}$ (**5**) was isolated after precipitation from the mixture by using hexanes. Analysis by NMR is consistent with a paramagnetic species with signals that ranged from -33.9 to 51.9 ppm in the ^1H NMR spectrum and no signal in the ^{31}P NMR spectrum.^[35] Analysis by ATR-IR spectroscopy shows the disappearance of the $\text{C}=\text{O}$ band at 1651 cm^{-1} (see the Supporting Information, Figure S15). As in the case of the Ni^{I} analogue $(^{\text{Ph}}\text{dppb})\text{NiCl}$,^[15] the band has most likely shifted to lower energies, but its exact assignment is hampered by the presence of a large number of signals in the fingerprint region of

the IR spectrum. The structure of complex **5**, determined by single-crystal X-ray diffraction, is shown to be a distorted tetrahedral geometry around the iron center (Figure 4, Table 3), which incorporated both phosphine arms, a chloride ligand, and the ketone moiety. The $\text{C}=\text{O}$ bond length has elongated from $1.218(3)$ in complex **2** to $1.3296(14)$ in product **5**, which indicates the presence of backdonation from the Fe center to the ketone moiety. To the best of our knowledge, this compound is the first structurally characterized $\eta^2(\text{C},\text{O})$ -bound Fe^{I} complex. EPR measurements of complex **5** in toluene at 100 K show signals at $g = 1.97$, 3.13 , and 4.99 , which are typical for a

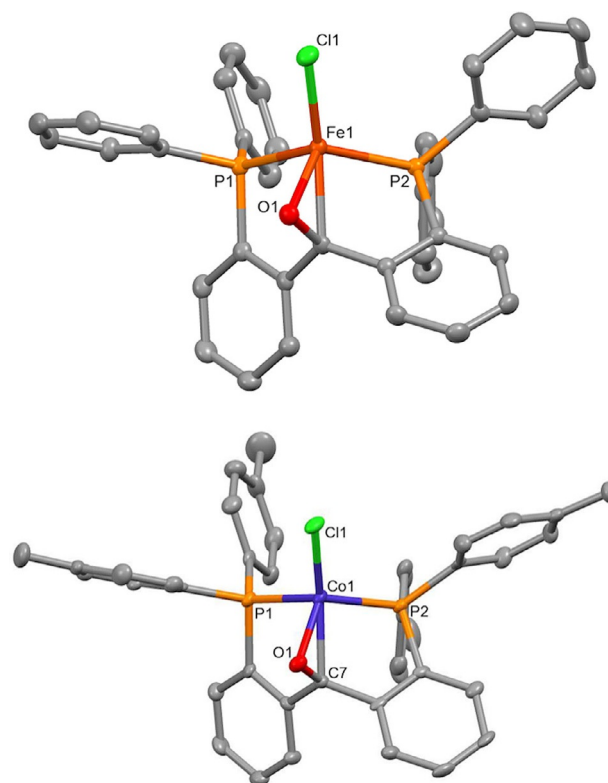


Figure 4. Top: X-ray crystal structure of $(^{\text{Ph}}\text{dppb})\text{FeCl}$ (**5**). Co-crystallized toluene molecule and hydrogen atoms are omitted for clarity; ellipsoids are shown at 50% probability level. Selected bond lengths (\AA) and angles ($^\circ$): $\text{Fe1}-\text{O1}$: $1.9072(8)$, $\text{Fe1}-\text{C7}$: $2.0881(12)$, $\text{C7}-\text{O1}$: $1.3296(14)$, $\text{Fe1}-\text{P1}$: $2.3992(3)$, $\text{Fe1}-\text{P2}$: $2.3559(3)$, $\text{Fe1}-\text{Cl1}$: $2.2328(3)$, $\text{P1}-\text{Fe1}-\text{P2}$: $106.350(12)$. Bottom: X-ray crystal structure of $(^{\text{Ptol}}\text{dppb})\text{CoCl}$ (**6pTol**). Hydrogen atoms are omitted for clarity, ellipsoids are shown at 50% probability level. Selected bond lengths (\AA) and angles ($^\circ$): $\text{Co1}-\text{O1}$: $1.947(3)$, $\text{Co1}-\text{C7}$: $2.071(5)$, $\text{C7}-\text{O1}$: $1.307(6)$, $\text{Co1}-\text{P1}$: $2.2908(14)$, $\text{Co1}-\text{P2}$: $2.3013(15)$, $\text{Co1}-\text{Cl1}$: $2.2072(15)$, $\text{P1}-\text{Co1}-\text{P2}$: $109.62(6)$.

Table 3. Selected bond lengths and angles for complexes **5**, **6pTol**, and **7**.

	$\text{C}=\text{O}$ [\AA]	$\text{M}-\text{O}$ [\AA]	$\text{M}-\text{C}$ [\AA]	PMP angle [$^\circ$]
$(^{\text{Ph}}\text{dppb})\text{FeCl}$, (5)	$1.3296(14)$	$1.9072(8)$	$2.0881(12)$	$106.350(12)$
$(^{\text{Ptol}}\text{dppb})\text{CoCl}$, (6pTol)	$1.307(6)$	$1.947(3)$	$2.071(5)$	$109.62(6)$
$(^{\text{Ph}}\text{dppb})\text{NiCl}$, (7) ^[15]	$1.310(2)$	$1.9740(15)$	$2.006(2)$	$107.57(2)$

high-spin Fe^{I} species with $S=3/2$ ($E/D=0.16$). A similar EPR spectrum was obtained by Harman and co-worker for a high-spin $\text{TpFe}(\text{I})-\text{N}_2$ species ($\text{Tp}=\text{tris}(\text{pyrazolyl})\text{borate}$) with signals at $g_{\text{eff}}=4.0$ and 2.0 , which was also assigned as an Fe^{I} species.^[36] The reduction of cobalt complex **3** was achieved in a similar manner and resulted in a paramagnetic species **6**; this was confirmed by its ^1H NMR spectrum, which displays signals that range from -12 to 32 ppm, and by the lack of signals in its ^{31}P NMR spectrum. The obtained IR spectrum is consistent with the aforementioned Fe^{I} and Ni^{I} complexes **5** and **7**: the intense $\text{C}=\text{O}$ band, which was observed at 1647 cm^{-1} in complex **3**, is shifted to a lower value within the fingerprint region. Magnetic susceptibility measurement by using Evans method resulted in a μ_{eff} value of $3.16\text{ }\mu_{\text{B}}$ ($n=2$), which is consistent with a high-spin Co^{I} complex ($S=1$). Crystals that were suitable for X-ray diffraction could not be obtained for complex **6**; instead, the structural determination was successful with the closely related analogue **6pTol** (Figure 4, bottom), and analysis of this complex confirmed the $\eta^2(\text{C},\text{O})$ coordination of the ketone moiety.

Moving further to the right of the transition series, complexation with copper(I) was investigated. A reaction of CuCl with $^{\text{Ph}}\text{dppb}$ in MeCN did not afford the analogous $\eta^2(\text{C},\text{O})$ complex; instead, it resulted in a dimeric copper complex $[(^{\text{Ph}}\text{dppb})\text{CuCl}]_2$ (**9**). X-ray single-crystal diffraction (Figure 5) revealed that complex **9** consists of two Cu atoms with a trigonal planar geometry that is bridged by the two diphosphine ligands, which each contribute one P atom to the coordination environment of each metal. The structure contains an inversion center, and this resulted in two different Cu–O distances of $2.9953(11)$ and $3.0529(12)\text{ }\text{\AA}$ and a C=O bond length of $1.2218(19)\text{ }\text{\AA}$, which indicates the absence of π coordination. This was confirmed by ATR-IR spectroscopy, in which a single, intense C=O band is visible at 1643 cm^{-1} . To understand why the Cu^{I} complex adopts a different coordination geometry from the previously

described ketone-bound complexes **5–7**, DFT calculations were performed on the putative monomeric Cu^{I} complex $(^{\text{Ph}}\text{dppb})\text{CuCl}$ at the B3LYP/TZVP level of theory (Table 4). Interestingly, it exhibits a bidentate binding mode analogous to

Table 4. Wiberg bond indices (WBI), natural charges (q), and natural spin densities (NSD) from calculated densities at the B3LYP/TZVP level for the ligand and mononuclear $(^{\text{Ph}}\text{dppb})\text{M}^{\text{I}}\text{Cl}$ complexes.

	1 ($^{\text{Ph}}\text{dppb}$)	5 (Fe^{I})	6 (Co^{I})	7 (Ni^{I})	Cu^{I}
WBI(C–O)	1.78	1.31	1.40	1.46	1.79
WBI(M–O)	–	0.38	0.31	0.24	< 0.01
WBI(M–C)	–	0.33	0.33	0.33	< 0.01
q(C)	0.56	0.21	0.27	0.29	0.55
q(O)	–0.52	–0.66	–0.62	–0.61	–0.49
q(C+O)	0.04	–0.45	–0.35	–0.32	0.06
NSD(M)	–	3.21	2.01	0.99	–
NSD(CO)	–	–0.34	–0.23	–0.14	–

that observed in compounds **2–4**, in which the $\text{C}=\text{O}$ moiety is not bound to the metal. Consequently, M–O and M–C WBIs below 0.01 are obtained, and the C–O WBI (1.79) as well as the corresponding NBO charge ($q(\text{C}+\text{O})=+0.06\text{ e}$) are close to those of the free ligand. The fact that a π -coordinating structure is less favored for the Cu complex is in line with the experimental observation of the dimeric structure of complex **9**. This is likely a consequence of d-orbital contraction along the transition series, which makes π backdonation less efficient for Cu^{I} , in accordance with the description of the $\text{C}=\text{O}$ moiety being mostly an electron-accepting ligand.

Discussion on the $\eta^2(\text{C},\text{O})$ binding mode of the ketone moiety

Complexes **5–7** constitute a unique series of $\eta^2(\text{C},\text{O})$ complexes with paramagnetic, first-row transition metals, and they provide an opportunity to investigate periodic trends in π bonding. First, the degree of activation of the C–O bond, as indicated by elongation of the C–O bond with respect to the free ligand ($1.213(3)\text{ }\text{\AA}$), is approximately the same for Ni ($1.310(2)\text{ }\text{\AA}$) and Co-based ($1.307(6)\text{ }\text{\AA}$) complexes and somewhat higher for the Fe complex ($1.3296(14)\text{ }\text{\AA}$). This is consistent with an increasing degree of π backdonation as the metal becomes less electronegative in the order Ni (1.91) to Fe (1.83). More strikingly, the ratio between the M–C and M–O bond lengths changed significantly along the series: the M–C bond shortens going from Fe to Ni (**5**: $2.0881(12)\text{ }\text{\AA}$, **7**: $2.006\text{ }\text{\AA}$), whereas the M–O distance increases (**5**: $1.9072(8)\text{ }\text{\AA}$, **7**: $1.974(3)\text{ }\text{\AA}$).

In complement of the above experimental data, DFT calculations were performed on compounds **5–7**. The optimized geometries for the $\eta^2(\text{C},\text{O})$ complexes **5–7** adequately reproduce the experimental data (see the Supporting Information, Table S1). The charge transfer increases from Ni to Fe, with the highest amount of charge transfer calculated for iron complex **5**, as seen in the total natural charge ($q(\text{C}+\text{O})$) on the C=O fragment (**5**: -0.45 , **6**: -0.35 , **7**: -0.32). This is further support-

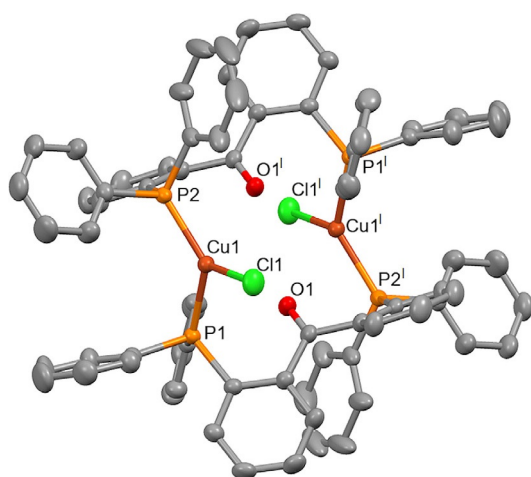


Figure 5. X-ray crystal structure of $[(^{\text{Ph}}\text{dppb})\text{CuCl}]_2$ (**9**). Structure contains a centrosymmetric point. Hydrogen atoms are omitted for clarity; the ellipsoids are shown at the 50% probability level. Selected bond lengths (\AA) and angles ($^\circ$): Cu1–O1: $2.9953(11)$, Cu1–O1': $3.0529(12)$, Cu1–P1: $2.2488(4)$, Cu1–P2': $2.2077(4)$, Cu1–Cl1: $2.2145(5)$, C7–O1: $1.2218(19)$, P1–Cu1–P2': $126.495(17)$. Symmetry code i : $1-x, 1-y, 1-z$.

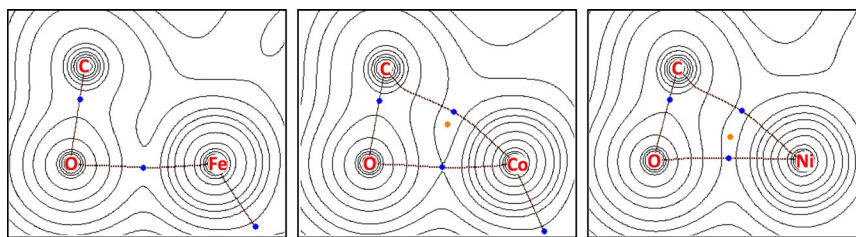


Figure 6. Electron density plots of the AIM calculations of complexes **5** (left), **6** (middle), and **7** (right). Bond critical points are given in blue, ring critical points are given in orange.

ed by an increase in the C–O WBI from Fe complex **5** to Ni complex **7** (**5**: 1.31, **6**: 1.40, **7**: 1.46), in accordance with the corresponding trend in C–O bond elongation. The M–C WBI is constant at 0.33 in complexes **5**–**7**, whereas the M–O WBI significantly decreases from 0.38 for complex **5** to 0.24 for **7**. In other words, the M–O bond becomes comparatively stronger as the extent of charge transfer to the C=O fragment increases.

More light was shed on the bonding situation by AIM analysis of complexes **5**, **6**, and **7** (Figure 6). The Ni complex **7** displays bond paths for both the M–C and the C–O interaction, with a corresponding ring critical point (rcp) that is close to equidistant from both bond critical points (bcp).^[37] In contrast, no M–C bond path, and consequently no rcp, is found in the Fe complex **5**. The Co complex **6** exhibits an intermediate situation, in which the rcp is close to the M–C bcp without complete merging.

Overall, the above computational and experimental data consistently indicate that moving along the first-row transition metal series from Ni^I to Fe^I results in complexes with 1) a higher degree of charge transfer to the C=O moiety and 2) an increase in the M–O contribution with a concomitant decrease in the M–C contribution to the bonding. These two trends may appear difficult to reconcile with the DCD model: as the degree of π backdonation increases, one would expect the M–C bond to *shorten*, because the accepting $\pi^*(\text{C}=\text{O})$ orbital has a larger coefficient on the carbon atom.^[18] Therefore, we propose a minor contribution of a third ketyl radical resonance structure^[38] (Scheme 1 C), which can be described as the interaction of a ketyl radical anion that is strongly coupled to a high-spin M^{II} center. An increasing, but small, contribution of resonance structure C to the overall bonding from Ni to Fe is consistent with both the higher activation of the C–O bond and the decrease in M–C bonding, which is complemented with a stronger ionic M–O bonding with the more electropositive metal.

Some extent of spin separation is also apparent in the qualitative molecular orbital diagrams calculated for compounds **5** (Figure 7), **6**, and **7** (see the Supporting Information, Figures S40–S42). Of the five MOs of d parentage found for the Fe^I complex **5**, three are singly occupied and one is doubly occupied (α/β overlap: $S=0.99$). The last MO displays some spin separation, that is, the α and β spin orbitals overlap to a lesser extent: while both can be described as a bonding combination of a d orbital with the accepting $\pi^*(\text{C}=\text{O})$ orbital, the β spin or-

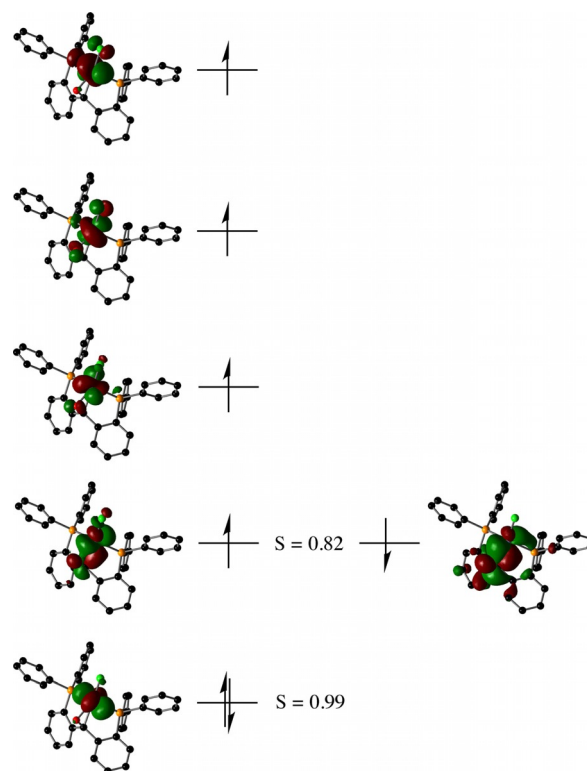


Figure 7. Qualitative molecular orbital diagram of complex **5**.

bitals display a somewhat higher ligand character. The observed overlap integral ($S=0.82$) is too large for the spin-separated resonance structure C (Scheme 1) to be considered as the best description of complex **5**, and it suggests only a minor contribution of the ketyl radical resonance structure. In agreement with other observations (see above), this lower degree of orbital overlap is found in the Fe^I complex **5** and to a much lesser degree in the Co^I ($S=0.92$) and Ni^I complexes ($S=0.97$), for which the contribution of resonance structure C is close to negligible. This interpretation is also consistent with the decreasing amount of calculated β spin density from 0.34 to 0.14 e in complexes **5** and **7**, respectively (Table 4, NSD(CO)).

Spin-separated electronic structures are widely accepted to be a good representation of reduced complexes that feature redox non-innocent σ -ligands, such as imines and pyridines, which can accept an electron in a remote π^* orbital.^[1,39–44] Such structures typically display low overlap integrals ($S<0.5$) between the relevant α and β orbitals. In contrast, the overlap

integrals are much higher for the series of complexes described herein, which is consistent with mostly covalent DCD bonding, with a minor contribution of the ketyl radical resonance structure in the case of Fe complex **5**.

Conclusions

The coordination chemistry of the diphosphine-ketone ligand ^{Ph}dpbp with first-row transition metals (M = Fe, Co, Ni, Cu) in the +II and +I formal oxidation states was investigated. The C=O moiety can adopt several binding modes, that is, non-bound in the M^{II} (M = Fe, Co, Ni) and Cu^I complexes, η¹(O) in the Ni^{II} cation, and η²(C,O) in the M^I complexes (M = Fe, Co, Ni).

The latter structures can be described as intermediates between a π complex and a metallaepoxide, in accordance with the Dewar–Chatt–Duncanson model. Geometric changes in the M^I complexes were observed to follow a periodic trend from Ni to Fe, that is, lengthening of the M–C bond with concomitant shortening of the M–O bond and a slight increase of the C=O bond length. This somewhat unexpected trend suggests a minor contribution of the ketyl radical resonance structure (C–O)^{•–}–M^I to the bonding in the case of Fe, which was corroborated by DFT calculations. These results contribute to a better understanding of the binding of π ligands to high-spin first-row transition-metal centers and will be of use for the design and mechanistic understanding of catalytic cycles that involve such species.

Experimental Section

General considerations

All reagents were purchased from commercial sources and used as received unless stated otherwise. All reactions were performed in a N₂ glovebox at room temperature unless stated otherwise. Deuterated benzene (C₆D₆) and deuterated dichloromethane (CD₂Cl₂) were degassed by using the freeze-thaw-pump method (4×) and subsequently stored over molecular sieves. Dichloromethane (CH₂Cl₂) was distilled over calcium hydride, and tetrahydrofuran (THF) was distilled over sodium/benzophenone before use; both solvents were degassed by bubbling N₂ through them for 30 min and stored over molecular sieves. Dry diethyl ether (Et₂O), hexanes, acetonitrile (MeCN), and toluene (C₇H₈) were acquired from a MBRAUN MB SPS-80 solvent purification system and further dried over molecular sieves before use. MeCN was filtered over alumina prior to use. NaBAR₄ was purchased and further dried under high vacuum for three days at 50 °C. CuCl was dried following standard procedures.^[45] ^{Ph}dpbp and (^{Ph}dpbp)NiCl₂ were synthesized by following literature procedures.^[15]

¹H, ¹¹B, ¹³C, ¹⁹F, and ³¹P NMR spectra were recorded on an Agilent MRF400 (¹H, ¹³C, ³¹P) or a Varian AS400 spectrometer (¹H, ¹¹B, ¹³C, ¹⁹F, ³¹P) at 25 °C and 400, 128, 100, 376, and 161 MHz, respectively. ¹H and ¹³C NMR chemical shifts are reported in ppm relative to TMS by using the residual solvent resonance as the internal standard. ¹¹B NMR chemical shifts are reported in ppm and externally referenced to BF₃·OEt₂. ³¹P NMR chemical shifts are externally referenced to 85% aqueous H₃PO₄. ¹⁹F NMR chemical shifts are externally referenced to CFCl₃. Infrared spectra were recorded on a PerkinElmer Spectrum One FT-IR spectrometer equipped with a general liquid cell accessory under a N₂ flow. UV/Vis spectra were mea-

sured on a Lambda 35 UV/Vis spectrometer. The UV/Vis samples were prepared under a N₂ atmosphere and sealed with a Teflon cap, and the spectra were recorded directly. EPR analyses were carried out by dissolving several milligrams of the compound in an appropriate solvent under inert conditions followed by filtration of the sample to ensure no solids were present. EPR spectra were recorded on a Bruker EMX Plus 6000 Gauss machine with ER 041 XG X-Band Microwave Bridge. ESI-MS spectra were recorded on a Waters LCT Premier XE KE317 Micromass Technologies spectrometer. Compounds for which elemental analysis is reported were either recrystallized or precipitated and dried under high vacuum overnight before submission.

Synthesis

^{pTol}dpbp: *o*-bromophenyl-di-*p*-tolyl-phosphine (4.93 g, 13.4 mmol) was suspended in Et₂O (30 mL). The light yellow suspension was cooled to –50 °C by using an acetone ice bath. *n*BuLi (1.6 M in hexane, 16 mmol, 10 mL) was added dropwise while the reaction was stirred, which resulted in a rapid color change from yellow to brown. Within 30 min, the reaction mixture was allowed to warm to RT and was directly cooled down to –50 °C again, after which a solution of *N,N*-dimethylcarbamoylchloride (0.61 mL, 6.5 mmol) in Et₂O (15 mL) was added dropwise over 20 min. During the addition, the temperature of the bath was kept between –35 and –45 °C, after which the suspension was stirred overnight and allowed to warm up to RT. The reaction was cooled again to 0 °C and treated with an aqueous solution of NH₄Cl (2.5 M, 38 mL, 4.5 g, 85 mmol), which turned the suspension orange-yellow. The mixture was washed with Et₂O, the combined organic phases were dried with MgSO₄, and the solvents were evaporated. The obtained sticky yellow compound was washed with MeOH, and the solvent was removed by evaporation to give the product as a yellow powder (2.41 g, 4.0 mmol, 61%). ¹H NMR (C₆D₆): δ_H = 7.37 (t, *J* = 7.6 Hz, 8H), 7.37 (m, 2H), 7.31 (dd, *J* = 7.7, 2.4 Hz, 2H), 6.95 (td, *J* = 7.5, 1.1 Hz, 2H), 6.91 (d, *J* = 7.7 Hz, 8H), 6.83 (td, *J* = 7.5, 1 Hz, 2H), 2.03 ppm (s, 12H); ³¹P NMR (C₆D₆): δ_P = –9.77 ppm; ¹³C NMR (CDCl₃): δ_C = 197.35 (t, *J* = 3 Hz), 144.64 (dd, *J* = 24.4, 1 Hz), 140.68 (*J* = 26.1, 2.2 Hz), 138.21, 135.56 (dt, *J* = 3, 11 Hz), 135.00, 134.45 (m), 131.03 (t, *J* = 3.3 Hz), 130.66, 129.48 (m), 128.00, 21.21 ppm; ATR-IR: $\tilde{\nu}$ = 3012, 2956, 2920, 2863, 1910, 1738, 1664, 1598, 1495, 1446, 1395, 1296, 1271, 1243, 1185, 1090, 1018, 928, 805, 747, 637, 507 cm^{–1}; HRMS (ESI, MeCN AgNO₃/H₂O): *m/z* calcd for C₈₂H₇₂O₂P₂Ag: 1319.3534 [2M+Ag]⁺; found: 1319.3529; elemental analysis calcd (%) for C₄₁H₃₆OP₂: C 81.17, H 5.98; found: C 80.84, H 6.05.

(^{Ph}dpbp)FeCl₂ (**2**): FeCl₂·1.5THF (38.1 mg, 0.162 mmol) was suspended in CH₂Cl₂ (2 mL) in a vial in the glovebox at RT. ^{Ph}dpbp (89.2 mg, 0.162 mmol) was dissolved in CH₂Cl₂ (2 mL) in a separate vial. After stirring both mixtures for 10 min, the ligand solution was added to the Fe precursor; this resulted in a yellow suspension that turned to yellow-brown after 10 min. The mixture was stirred overnight, after which all volatiles were removed in vacuum. The obtained solids were precipitated from THF/hexanes (1:4) and isolated by filtration. The product was extracted with THF, and the organic phases were dried in vacuum to give product **2** as a pale brownish-yellow solid (95.7 g, 0.141 mmol, 87%). ¹H NMR (CD₂Cl₂): δ_H = 30.85, 16.04, 14.17, 12.51, 8.32, 7.36, 6.50, 3.90, 2.84, 1.92, 1.25, 0.85, 0.09, –1.31, –5.74 ppm; ATR-IR: $\tilde{\nu}$ = 3055, 1650, 1584, 1561, 1482, 1435, 1302, 1283, 1095, 930, 747, 691, 635, 495 cm^{–1}; UV/Vis: λ_{max} = 400 nm; HRMS (ESI, THF) *m/z* calcd for FeClC₃₇H₂₈OP₂: 641.0654 [M–X]⁺; found: 641.0737; elemental analysis calcd (%) for FeCl₂C₃₇H₂₈OP₂ (677.32 g/mol): C 65.61, H 4.17; found: C 64.96, H 4.07.

(^{Ph}dppb)CoCl₂ (3): CoCl₂ (23.9 mg, 0.184 mmol) was suspended in Et₂O (1 mL) in a vial in the glovebox at RT. ^{Ph}dppb (100.8 mg, 0.183 mmol) was dissolved in Et₂O (6 mL) in a separate vial. After stirring both mixtures for 10 min, the ligand suspension was added to the Co precursor, which resulted in a green suspension. The mixture was stirred overnight, after which all volatiles were removed in vacuum. The obtained solids were precipitated from THF/hexanes (1:3) and isolated by filtration. The product was extracted with THF, and the organic phases were dried in vacuum to give product **3** as a green solid (103 mg, 0.152 mmol, 83%). ¹H NMR (CD₂Cl₂): δ_H=18.68, 13.71, 11.76 (minor), 10.13, 8.00, 7.31, 7.22, 7.12, 1.26 (minor), 0.94, 0.08, −0.56, −3.73 ppm (broad); ATR-IR: ν̄=3051, 1647, 1482, 1435, 1284, 1254, 1166, 1126, 1095, 930, 769, 748, 740, 634, 522, 511, 497, 471 cm^{−1}; UV/Vis: λ_{max}=648, 737 nm; HRMS (ESI, MeCN) *m/z* calcd for CoClC₃₇H₂₈OP₂: 644.0636 [M−Cl]⁺, CoClC₃₉H₃₁OP₂N: 685.0901 [M−Cl+MeCN]⁺; found: 644.0635, 685.0905; elemental analysis calcd (%) for CoClC₃₇H₂₈OP₂ (680.40 g/mol): C 65.31, H 4.15; found: C 64.87, H 4.03.

(^{Ph}dppb)FeCl (5): Naphthalene (141.2 mg, 1.1 mmol) was dissolved in THF (20 mL) in the glovebox at RT. A lump of Na⁰ was added and the mixture was stirred for 3 h to give a dark green solution. FeCl₂ (115.3 mg, 0.909 mmol) was suspended in THF (8 mL) in a vial, and ^{Ph}dppb (500.2 mg, 0.908 mmol) was dissolved in another vial in THF (12 mL). The FeCl₂ suspension was cooled to −78 °C and stirred for 10 min; the dissolved ligand was added and the resulting mixture was stirred for 15 min. The naphthalide solution was filtered and added to the cooled mixture over 15 min. This final mixture was stirred at −78 °C for 1 h and then at RT for 18 h, and it was then concentrated in vacuum to a total volume of 10 mL. A brown precipitate was obtained after the addition of hexanes (50 mL), which was collected by filtration. The product was extracted with THF, and the organic phases were dried in vacuum to give pure product **5** (0.566 g, 0.882 mmol, 97%). ¹H NMR (CD₂Cl₂): δ_H=52.08, 33.93, 11.87, 11.12, 3.83, 0.30, −1.30, −5.74, −6.38, −13.24, −33.76; ATR-IR: ν̄=2962, 1725, 1658, 1584, 1480, 1435, 1262, 1117, 1099, 1003, 928, 817, 742, 692, 542, 502 cm^{−1}; UV/Vis: λ_{max}=480 nm;

(^{Ph}dppb)CoCl (6): Naphthalene (27.9 mg, 0.218 mmol) was dissolved in THF (2 mL) in the glovebox at RT. A lump of Na⁰ was added, and the mixture was stirred for 3 h, after which a dark green solution was obtained. CoCl₂ (23.7 mg, 0.182 mmol) was suspended in THF (1 mL) in a vial, and ^{Ph}dppb (100.1 mg, 0.182 mmol) was dissolved in THF (3 mL) in a separate vial, and both mixtures were stirred for 10 min. The ligand solution was added to the Co suspension, and the resulting mixture was cooled to −78 °C and stirred for 45 min. The naphthalide solution was filtered and added to the cooled mixture in 45 min. This final mixture was stirred for a further 1.5 h at −78 °C and then for 18 h at RT; the resultant mixture was concentrated in vacuo to a volume of ca. 1.5 mL. Hexane was added (5 mL) and the solids were collected by filtration. The product was extracted with THF, and the organic phases were dried in vacuum, which resulted in product **6** as a brown solid (74.5 mg, 0.109 mmol, 60%). ¹H NMR (C₆D₆): δ_H=20.38, 14.24, 13.68, 3.57, 1.41, 1.25, 0.89, 0.06, −1.42, −2.37, −6.59, −8.10, −9.49, −16.73 ppm; ATR-IR: ν̄=3054, 1585, 1481, 1460, 1435, 1241, 1160, 1133, 1096, 1069, 1027, 998, 918, 878, 847, 776, 743, 691, 657, 623, 581, 543, 517, 501, 480 cm^{−1}; UV/Vis: λ_{max}=448, 530, 660 nm.

(^{pTol}dppb)CoCl (6^{pTol}): This compound was synthesized by using an analogous procedure to the synthesis of compound **6**, which gave product **6^{pTol}** in a yield of 86% (300.3 mg, 0.43 mmol). ¹H NMR (C₆D₆): δ_H=31.59, 20.00, 17.64, 14.34, 13.54, 9.21, −0.06, −0.98 (broad), −6.07, −7.97, −16.38 ppm; ATR-IR: ν̄=2919, 2863,

1599, 1498, 1434, 1397, 1258, 1241, 1189, 1096, 1019, 917, 803, 777, 693, 626, 510 cm^{−1}; UV/Vis: λ_{max}=525 nm; elemental analysis calcd (%) for C₄₁H₃₆Cl₂FeOP₂ (733.42 g/mol): C 70.24, H 5.18; found: C 70.00, H 5.37.

[Ni(^{Ph}dppb)(μ-Cl)]₂(BAr^F)₄ (8): (^{Ph}dppb)NiCl₂ was suspended in Et₂O (0.5 mL) in a vial in the glovebox. NaB(Ar^F)₄ was also suspended in Et₂O (2 mL) and transferred to the [Ni] mixture. The final mixture was stirred overnight at room temperature, then all solvents were removed in vacuo. Et₂O (1 mL) and hexanes (3 mL) were added, and the formed precipitation was isolated by filtration and washed with hexanes (3×1 mL). The product was extracted with Et₂O (3 mL), and the solvents were removed in vacuum to give product **9** as a brown powder (89%, 31.5 mg, 0.0104 mmol). ¹H NMR (CD₂Cl₂): δ_H=8.04 (t, *J*=7.6 Hz), 7.93 (t, *J*=7.6 Hz), 7.80 (d, *J*=7.4 Hz), 7.77 (d, *J*=5.0 Hz), 7.73 (m, broad, BAr^F₄), 7.62 (q) 7.58 (d, *J*=7.6 Hz), 7.56 (s, BAr^F₄), 7.49 (t, *J*=7.7 Hz), 7.43 (t, *J*=7.6 Hz), 7.37 (m), 7.25 (t, *J*=7.7 Hz; s, broad, 1H), 7.14 (t, *J*=7.6 Hz), 7.07 (t, *J*=7.7 Hz), 6.95 (t, *J*=7.9 Hz), 6.89 (s, broad, 1H), 6.33 (d, 1H, *J*=7.9 Hz), 6.04 ppm (s, broad, 1H); ¹³C NMR (CD₂Cl₂): δ_C=206.83 (t, *J*_{CP}=2.9 Hz), 162.14 (q, *J*_{CB}=49.2 Hz), 140.94 (t, *J*=5.7 Hz), 140.28 (t, *J*=3.6 Hz), 138.26 (t, *J*=18.8 Hz), 137.47 (t, *J*=3.2 Hz), 137.01 (t, *J*=4.0 Hz), 136.68 (q, *J*=4.0 Hz), 136.47 (t, *J*=5.1 Hz), 135.90 (s), 135.48 (t, *J*=5.1 Hz), 135.20 (s), 134.83 (s), 134.50 (s), 133.94 (s), 133.74 (t, *J*=5.8 Hz), 132.80 (s), 132.06 (s), 130.34 (t, *J*=5.7 Hz), 130.01 (s), 129.59 (t, *J*=4.9 Hz), 129.42 (q, *J*=2.8 Hz), 129.10 (m), 128.87 (t, *J*=4.9 Hz), 128.60 (s), 128.39 (s), 127.46 (t, *J*=25.6 Hz), 126.34 (s), 120.93 (s), 120.29 (s), 119.77 (s), 118.73 (s), 117.89 (septet, *J*=3.9 Hz), 103.36 (s), 66.20 ppm (s); ³¹P NMR (CD₂Cl₂): δ_P=36.38, 5.58 ppm; ¹¹B NMR (CD₂Cl₂): δ_B=−6.64 ppm; ¹⁹F NMR (CD₂Cl₂): δ_F=−62.86 ppm; ATR-IR: ν̄=1610, 1571, 1525, 1439, 1354, 1273, 1115, 886, 839, 744, 712, 681, 474 cm^{−1}; HRMS (ESI, MeCN): *m/z* calcd for NiClC₃₇H₂₈OP₂: 643.0657 [M−NiCl]⁺ (monomer); found: 643.0549; elemental analysis calcd (%) for C₁₃₈H₈₀B₂Cl₂F₄₈Ni₂O₂P₄ (3015.84 g/mol): C 54.96, H 2.67; found: C 54.70, H 2.72.

[^{Ph}dppb)CuCl]₂ (9): Anhydrous CuCl (8.7 mg, 0.088 mmol) was dissolved in MeCN (0.5 mL) in a vial in the glovebox at RT. ^{Ph}dppb (48.4 mg, 0.092 mmol) was dissolved in MeCN (10 mL) in a separate vial. After stirring both mixtures for 10 min, the CuCl solution was slowly added to the ligand solution, and the mixture was directly filtered through a pipette filter into a new vial. The mixture was left standing for 48 h, after which orange/brown crystals were formed. The MeCN was removed by decantation, the crystals were washed with MeCN (2×1 mL), and all residual solvents were removed in vacuum, which resulted in product **8** as a crystalline material (35 mg, 0.027 mmol, 61%). ¹H NMR (CD₂Cl₂): δ_H=7.40, 7.34, 7.02, 1.98, 1.28, 0.87, 0.43 ppm; ³¹P NMR (CD₂Cl₂): δ_P=−12.19 ppm; ATR-IR: ν̄=3049, 1643, 1584, 1561, 1479, 1435, 1300, 1266, 1254, 1167, 1125, 1094, 929, 744, 694, 639, 525, 493 cm^{−1}; UV/Vis: λ_{max}=400, 890 nm; HRMS (ESI, MeCN) *m/z* calcd for Cu₂C₇₄H₅₆ClO₂P₄: 1263.1510 [M−Cl]⁺; found: 1263.1427, C₃₉H₃₁CuOP₂N: 654.1177 [M−CuLCl−Cl+MeCN]⁺ (monomer); found: 654.1066; elemental analysis calcd (%) for Cu₂C₇₄H₅₆Cl₂O₂P₄ (1299.12 g/mol): C 68.42, H 4.35; found: C 69.12, H 4.32.

DFT

DFT calculations were performed on the Gaussian 09 software package^[46] by using the B3LYP (Becke, three-parameter, Lee–Yang–Parr) functional and the TZVP basis set on all atoms, except for the calculations of compound **9**, which were performed with the B3LYP functional and the 6-31 g** basis set. The structures were optimized without any symmetry restraints. Frequency analyses

were performed on all calculations to verify that the obtained stationary points were in fact minima. For qualitative MO diagrams, the canonical orbitals were biorthogonalized to maximize alignment of electron pairs. For NBO calculations, the NBO6 program up to the NLMO basis set was used.^[47] AIM calculations^[20] were performed, and corresponding pictures were generated by using the Multiwfn program.^[48]

Acknowledgements

We thank Jochem Blum for synthetic assistance, Dr. Johann Jastrzebski for assistance with NMR analysis, and Dr. Pradip Ghosh for assistance with the MO diagram calculations. D.V. and M.E.M. would like to thank the Sectorplan Natuur- en Scheikunde (Tenure-track grant at Utrecht University) for financial support. The X-ray diffractometer was financed by The Netherlands Organization for Scientific Research (NWO). This work was sponsored by NWO Exacte en Natuurwetenschappen (Physical Sciences) for the use of supercomputer facilities, with financial support from the Nederlandse Organisatie voor Wetenschappelijk Onderzoek (Netherlands Organization for Scientific Research, NWO).

Conflict of interest

The authors declare no conflict of interest.

Keywords: coordination modes • density functional calculations • ketones • pi ligands • transition metals

- [1] P. J. Chirik, *Angew. Chem. Int. Ed.* **2017**, *56*, 5170–5181; *Angew. Chem.* **2017**, *129*, 5252–5265.
- [2] B. Marciniec, H. Maciejewski, C. Pietraszuk, P. Pawluc, *Hydrosilylation: A Comprehensive Review on Recent Advances*, Springer, Dordrecht, **2009**.
- [3] E. P. Kundig, *Transition Metal Arene pi-Complexes in Organic Synthesis and Catalysis*, Springer, Berlin, **2004**.
- [4] D. G. A. Verhoeven, M.-E. Moret, *Dalton Trans.* **2016**, *45*, 15762–15778.
- [5] S. H. Bertz, R. A. Hardin, T. J. Heavey, C. A. Ogle, *Angew. Chem. Int. Ed.* **2013**, *52*, 10250–10252; *Angew. Chem.* **2013**, *125*, 10440–10442.
- [6] A. V. R. Madduri, S. R. Harutyunyan, A. J. Minnaard, *Angew. Chem. Int. Ed.* **2012**, *51*, 3164–3167; *Angew. Chem.* **2012**, *124*, 3218–3221.
- [7] K. Mikami, K. Wakabayashi, K. Aikawa, *Org. Lett.* **2006**, *8*, 1517–1519.
- [8] Q. Jing, C. A. Sandoval, Z. Wang, K. Ding, *Eur. J. Org. Chem.* **2006**, 3606–3616.
- [9] K. Ruhland, A. Obenhuber, S. D. Hoffman, *Organometallics* **2008**, *27*, 3482–3495.
- [10] A. Obenhuber, K. Ruhland, *Organometallics* **2011**, *30*, 4039–4051.
- [11] A. Obenhuber, K. Ruhland, *Organometallics* **2011**, *30*, 171–186.
- [12] L. E. Doyle, W. E. Piers, J. Borau-Garcia, *J. Am. Chem. Soc.* **2015**, *137*, 2187–2190.
- [13] L. E. Doyle, W. E. Piers, J. Borau-Garcia, M. J. Sgro, D. M. Spasyuk, *Chem. Sci.* **2016**, *7*, 921–931.
- [14] L. E. Doyle, W. E. Piers, D. W. Bi, *Dalton Trans.* **2017**, *46*, 4346–4354.
- [15] B. W. H. Saes, D. G. A. Verhoeven, M. Lutz, R. J. M. Klein Gebbink, M.-E. Moret, *Organometallics* **2015**, *34*, 2710–2713.
- [16] G. J. Kubas, *J. Organomet. Chem.* **2001**, *635*, 37–68.
- [17] R. H. Crabtree, *The organometallic chemistry of the transition metals*, 6th ed., Wiley, Hoboken, **2014**.
- [18] T. A. Albright, R. Hoffmann, J. C. Thibault, D. L. Thorn, *J. Am. Chem. Soc.* **1979**, *101*, 3801–3812.
- [19] The magnetic susceptibility by Evans method could not be determined for complex **2** owing to solubility issues.
- [20] R. F. W. Bader, *Chem. Rev.* **1991**, *91*, 893–928.
- [21] As described in ref. [15], the crystals compound **4** were in two forms: **4** and **4-CH₂Cl₂**. This led to slight changes in the reported distances between the two compounds (Table 1, **4**). The values for **4-CH₂Cl₂** are the following: C=O 1.223(4), O–M 3.092(2) Å, PMP angle 113.76(3)°.
- [22] J. I. van der Vlugt, E. A. Pidko, D. Vogt, M. Lutz, A. L. Spek, A. Meetsma, *Inorg. Chem.* **2008**, *47*, 4442–4444.
- [23] B. J. Barrett, V. M. Iluc, *Inorg. Chem.* **2014**, *53*, 7248–7259.
- [24] D. L. Coombs, S. Aldridge, C. Jones, D. J. Willock, *J. Am. Chem. Soc.* **2003**, *125*, 6356–6357.
- [25] N. R. Bunn, S. Aldridge, D. L. Kays, N. D. Coombs, A. Rossin, D. J. Willock, J. K. Day, C. Jones, L.-I. Ooi, *Organometallics* **2005**, *24*, 5891–5900.
- [26] M. C. Bonnet, F. Dahan, A. Ecker, W. Keim, R. P. Schulz, I. Tkatchenko, *Chem. Commun.* **1994**, 615–616.
- [27] B. T. Rasley, M. Rapt, R. J. Kulawiec, *Organometallics* **1996**, *15*, 2852–2854.
- [28] C. P. Butts, J. Crosby, G. C. Lloyd-Jones, S. C. Stephen, *Chem. Commun.* **1999**, 1707–1708.
- [29] G. Sánchez, J. García, D. Meseguer, J. L. Serrano, L. García, J. Pérez, G. López, *Dalton Trans.* **2003**, 4709–4717.
- [30] G. Sánchez, J. García, J. J. Ayllón, J. L. Serrano, L. García, J. Pérez, G. López, *Polyhedron* **2007**, *26*, 2911–2918.
- [31] Z. J. A. Komon, G. C. Bazan, C. Fang, X. Bu, *Inorg. Chim. Acta* **2003**, *345*, 95–102.
- [32] M.-T. Chen, W.-Y. Lee, T.-L. Tsai, L.-C. Liang, *Organometallics* **2014**, *33*, 5852–5862.
- [33] D. J. Mindiola, R. Waterman, D. M. Jenkins, G. L. Hillhouse, *Inorg. Chim. Acta* **2003**, *345*, 299–308.
- [34] Y. Ganushevich, V. Miluykov, D. Yakhrov, O. Sinyashin, P. Lönnecke, E. Hey-Hawkins, *Inorg. Chim. Acta* **2011**, *376*, 118–122.
- [35] Attempts were made to perform spin multiplicity measurements following Evans method, but they failed owing to the low solubility of complex **5**.
- [36] A. McSkimming, W. H. Harman, *J. Am. Chem. Soc.* **2015**, *137*, 8940–8943.
- [37] G. Frenking, S. Shaik, *The Chemical Bond: The QTAI Perspective of Chemical Bonding* (Ed.: P. L. A. Popelier), Wiley-VCH, Weinheim, **2014**, Chap. 8, pp. 271–308. A bond critical point (BCP) is a saddle point in the electron density map at which the electron density decreases in two perpendicular directions and increases in the third direction. The bond path between two atoms is the path of maximal electron density that connects the BCP to the corresponding atoms. A ring critical point (RCP) describes the presence of a ring structure in the electron density map. It is also a saddle point in the electron density map: the electron density rises in two perpendicular directions and decreases in one.
- [38] J. F. Berry, *Chem. Eur. J.* **2010**, *16*, 2719–2724.
- [39] A. C. Bowman, C. Milsman, C. C. Hojilla Atienza, E. Lobkovsky, K. Wieghardt, P. J. Chirik, *J. Am. Chem. Soc.* **2010**, *132*, 1676–1684.
- [40] P. J. Chirik, K. Wieghardt, *Science* **2010**, *327*, 794–795.
- [41] B. de Bruin, E. Bill, E. Bothe, T. Weyhermüller, K. Wieghardt, *Inorg. Chem.* **2000**, *39*, 2936–2947.
- [42] D. G. H. Hetterscheid, J. Kaiser, E. Reijerse, T. P. J. Peters, S. Thewissen, A. N. J. Blok, J. M. M. Smits, R. de Gelder, B. de Bruin, *J. Am. Chem. Soc.* **2005**, *127*, 1895–1905.
- [43] D. G. H. Hetterscheid, M. Bens, B. de Bruin, *Dalton Trans.* **2005**, 979–984.
- [44] S. K. Russell, J. M. Hoyt, S. C. Bart, C. Milsman, S. C. E. Stieber, S. P. Sempron, S. DeBeer, P. J. Chirik, *Chem. Sci.* **2014**, *5*, 1168–1174.
- [45] W. L. F. Armarego, C. L. L. Chai, *Purification of Laboratory Chemicals* **2009**, Elsevier, Amsterdam, p. 470.
- [46] Gaussian 09 (Revision A.02), M. J. Frisch, G. W. Trucks, H. B. Schlegel, G. E. Scuseria, M. A. Robb, J. R. Cheeseman, G. Scalmani, V. Barone, B. Menonucci, G. A. Petersson, H. Nakatsuji, M. Caricato, X. Li, H. P. Hratchian, A. F. Izmaylov, J. Bloino, G. Zheng, J. L. Sonnenberg, M. Hada, M. Ehara, K. Toyota, R. Fukuda, J. Hasegawa, M. Ishida, T. Nakajima, Y. Honda, O. Kitao, H. Nakai, T. Vreven, J. A. Montgomery, Jr., J. E. Peralta, F. Ogliaro, M. Bearpark, J. J. Heyd, E. Brothers, K. N. Kudin, V. N. Staroverov, R. Kobayashi, J. Normand, K. Raghavachari, A. Rendell, J. C. Burant, S. S. Iyengar, J. Tomasi, M. Cossi, N. Rega, J. M. Millam, M. Klene, J. E. Knox, J. B. Cross, V. Bakken, C. Amado, J. Jaramillo, R. Gomperts, R. E. Stratmann, O. Yazyev, A. J. Austin, R. Cammi, C. Pomelli, J. W. Ochterski, R. L. Martin, K. Morokuma, V. G. Zakrzewski, G. A. Voth, P. Salvador, J. J. Dannenberg,

- S. Dapprich, A. D. Daniels, Ö. Farkas, J. B. Foresman, J. V. Ortiz, J. Cio-
slowski, D. J. Fox, Gaussian, Inc., Wallingford CT, **2009**.
- [47] NBO 6.0. E. D. Glendening, J. K. Badenhoop, A. E. Reed, J. E. Carpenter,
J. A. Bohmann, C. M. Morales, C. R. Landis, and F. Weinhold, Theoretical
Chemistry Institute, University of Wisconsin, Madison, WI, **2013**, [http://
nbo6.chem.wisc.edu/](http://nbo6.chem.wisc.edu/).

- [48] T. Lu, F. Chen, *J. Comput. Chem.* **2012**, *33*, 580–592.

Manuscript received: July 13, 2017

Accepted manuscript online: October 27, 2017

Version of record online: December 20, 2017